Wetting of chemically heterogeneous striped surfaces: Molecular dynamics simulations

Chinh Thanh Nguyen,[1] Murat Barisik,[2] and BoHung Kim[1,a]
[1]*School of Mechanical Engineering, University of Ulsan, Daehak-ro 93, Namgu, Ulsan 680-749, South Korea*
[2]*Department of Mechanical Engineering, Izmir Institute of Technology, Urla, Izmir 35430, Turkey*

(Received 18 October 2016; accepted 23 May 2018; published online 4 June 2018)

Using molecular dynamics simulations, we thoroughly investigated the wetting behaviors of a chemically heterogeneous striped substrate patterned with two different wetting materials, face-centered cubic gold and face-centered cubic silver. We analyzed the density distributions, normal stress distributions, surface tensions, and contact angles of a water droplet placed on the substrates at different heterogeneities. We found that the density and stress profile of the water droplet near the substrate-water interface were noticeably affected by altering the gold and silver contents in the substrate. Specifically, a greater portion of gold (more wetting) or smaller portion of silver (less wetting) in the substrate composition induced higher densities and higher normal stresses in the vicinity of the substrate surface. Also, it was observed that the surface tensions at liquid-vapor interface and solid-vapor interface were not largely impacted by the change of the substrate composition while the solid-liquid surface tension decreased exponentially with increasing fraction of gold. Most importantly, we found that contact angle of a nanometer-sized water droplet resting on the chemically heterogeneous striped substrate does not show linear dependence on corresponding surface fractions like that predicted by Cassie-Baxter model at the macro-scale. Consequently, we proposed a method for successfully predicting the contact angle by including the critical effects of the substrate heterogeneity on both surface tensions and line tension at the three-phase contact line of the water droplet and the chemically striped substrate. https://doi.org/10.1063/1.5031133

I. INTRODUCTION

The wetting behavior of solids is of great importance in many applications such as micro/nano-electro-mechanical systems (MEMS/NEMS), drug delivery mechanisms and devices, and nanoscale lubrication. Also, the thermal transport resistance at the solid-liquid interface between nanoscale device components is heavily influenced by the wettability of the solid.[1–6] A better understanding of the wetting behavior of fluids on solid substrates can help enhance the efficiency of such nano devices in terms of speed, accuracy, and size. Therefore, there has been significant research focused on investigating the wetting characteristics of a variety of solid substrates. Specifically, the wettability of chemically homogeneous flat solid substrates where the three-phase equilibrium of nano-droplets exists has been extensively investigated.[7–11]

In reality, solid substrates are not always chemically homogeneous but are chemically heterogeneous. In other words, the solid substrates can be comprised of several different materials in their structure rather than only one material. In these cases, the wetting behavior of the chemically heterogeneous substrates is assumed to be much more complicated than that of chemically pure substrates.

[a]Corresponding Author/E-mail: bohungk@ulsan.ac.kr, TEL: +82-52-259-2705 (BK)

Knowledge regarding the wetting characteristics of chemically heterogeneous surfaces has great applications ranging from inkjet printing, microchips, nanolithography, to protein hydration.[12–14] Theoretically, the wetting of a chemically heterogeneous flat surface is characterized by an apparent contact angle described by the Cassie-Baxter (CB) model.[15,16] For cases where composite surfaces contain only two different materials, the CB model can be written as follows.

$$\cos\theta_C = f_1 \cos\theta_{Y1} + f_2 \cos\theta_{Y2}, \tag{1}$$

where θ_C is the apparent contact angle; θ_{Y1} and θ_{Y2} are the equilibrium Young contact angles for the material 1 and material 2, respectively, and f_1 and f_2 are the surface fractions of material 1 and material 2, respectively. The Young contact angle for a droplet on a solid substrate is described by Young's equation:

$$\gamma_{SV} = \gamma_{SL} + \gamma_{LV} \cos\theta_Y, \tag{2}$$

where γ_{SV}, γ_{SL}, and γ_{LV} are the solid-vapor, solid-liquid, and liquid-vapor surface tensions at the boundaries between the solid-vapor, solid-liquid, and liquid-vapor interfaces, respectively, and θ_Y is the Young or macroscopic contact angle of a droplet. The CB model was derived by assuming linear additivity of the wetting free energies of the comprising materials and it is a generalized Young's equation for composite surfaces. Also, the model presumes that a water droplet stays on the top of structured solid surfaces and it is valid for any heterogeneity with length scales smaller than the size of the droplet.

Over the past decade, significant studies have been carried out to investigate the applicability of CB model for chemically heterogeneous surfaces. At the macro-scale, there have been noticeable studies confirming the validity of CB model in predicting the contact angles of droplets resting on chemically heterogeneous substrates.[17–22] At the nanoscale, Lundgren *et al.* reported that the contact angle of a liquid droplet whose radius is much larger than the width of rectangular islands or stripes of a chemically heterogeneous surface matches the CB model well.[23] However, Halverson later *et al.* proved that the contact angle of a chemically heterogeneous surface does not match the CB model while the Israelachvili-Gee model better predicts the contact angle of this kind of surface at the nanoscale.[24,25] Besides, Wang *et al.* demonstrated that positive as well as negative deviations from the linear additivity of contact angle can be observed for nano-droplets on chemical heterogeneous surfaces. This kind of nonlinear behavior was proved to be caused by the uneven exposure of mixture components to the solvent due to steric shielding when there is sufficient difference between polarities of mixture components.[26] Although recent results relevant to the wetting behavior of a chemically heterogeneous surface have been obtained, thorough comprehension of the wetting characteristics of chemically heterogeneous surfaces at the nanoscale has not yet been achieved. Therefore, based on the current understanding of the wetting behaviors of chemically heterogeneous surfaces, especially the concern of the validity of the CB model at the nanoscale, the objective of this research was to conduct a thorough investigation of the issue by analyzing the density distribution, normal stress distribution, surface tensions, and contact angle of a water droplet resting on a chemically heterogeneous striped substrate. Interestingly, this research attempted to propose a mathematical model to predict the contact angle of chemically heterogeneous striped surfaces patterned with two different materials at the nanoscale based on the pattern parameters.

This paper is organized as follows. In Section II, we provide the details of the MD simulations including a description of the simulation domains and methods. Also, the theoretical background for the research is introduced. In Section III, we discuss the density distribution, normal stress distribution, surface tensions evolution. In addition, the comparison between the contact angles obtained from MD simulations and the prediction values from Young's equation, Cassie-Baxter model, and the proposed model is provided. Finally, the conclusions of this study are summarized in Section IV.

II. SIMULATIONS AND METHODS

In this research, the chemically heterogeneous striped substrate was composed of face-centered cubic (FCC) gold (Au) and FCC silver (Ag). Gold and silver were chosen for constructing this type of chemically heterogeneous striped substrates because they have very similar lattice constants, 4.08 Å for gold and 4.086 Å for silver, which can help to build a stable structure of a chemically

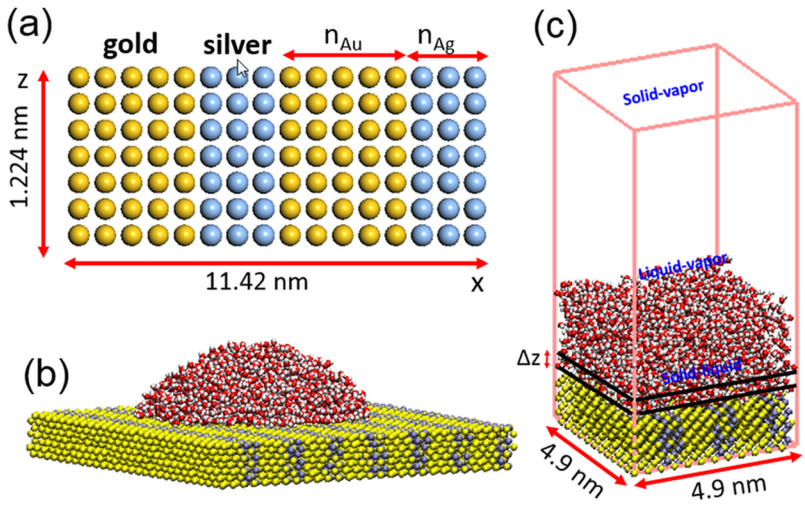

FIG. 1. Side-view schematic of a typical gold-silver striped substrate used in the simulations (a). Three-dimensional snapshot of a typical gold-silver-water system used in contact angle measurement (b). Schematic for a typical gold-silver-water system used in the density, stress, and surface tension calculation (c).

heterogeneous striped substrate. The period of substrate heterogeneity is 8 rows of gold or silver lattices. Also, due to the difference in the atomic radii of silver (1.65 Å) and gold (1.74 Å) is very small (0.09 Å) as compared to the atomic radius of an oxygen atom (0.48 Å), there are no cavities on the substrate surface such that any single water molecule can get stuck inside. Therefore, the composite FCC surfaces can be treated as flat. Fig. 1(a) shows a typical two-dimensional structure of the gold-silver striped substrate. Due to the sub-nanometer size of the stripes and the almost equal distance between the adjacent lattices of gold-gold, silver-silver, and gold-silver, the width of a gold or silver stripe was determined by the number of lattices constituting the stripe. Also, the surface fraction, denoted as f, was used to represent the chemical portions of gold and silver in the substrate with $f_{Au} = \frac{n_{Au}}{n_{Au}+n_{Ag}}$, $f_{Ag} = \frac{n_{Ag}}{n_{Au}+n_{Ag}}$, and $f_{Au} + f_{Ag} = 1$. The surface fractions of gold or silver evaluated were 0.125, 0.25, 0.375, 0.5, 0.625, 0.75, and 0.875.

For measuring contact angles of the droplets on the structurally different gold-silver substrates using MD simulations, a simulation domain was set up in which the dimensions are 11.42 nm in the x, y, and z directions as shown in Fig. 1(a, b). These dimension values were chosen large enough so that the water droplet will not move out of the substrate border due to diffusion. In addition, a second set of MD simulation was also used to calculate the density distribution, stress distribution, and surface tensions at the solid/water, solid/vapor and water/vapor interfaces. In this case, a thin water slab extending through periodic boundary conditions was placed on the solids. The simulation box is 4.9 nm in the x and y directions (parallel to the solid surface) and 10 nm in the z direction as shown in Fig. 1(c). This method was used to avoid finite-size effects which can occur if the data are collected directly from the simulations of the droplets formed on the substrates.

Two thousand H_2O molecules were used to represent a water droplet in the contact angle measurement simulations as well as in density, stress, and surface tension calculation simulations. This number of water molecules is adequate to represent a water droplet at the nanoscale and can help to save computational cost because a greater number of water molecules does not significantly affect the contact angle value.[10] The TIP4P/2005 model was chosen for water molecules because it can provide correct results for the orthobaric density and surface tensions.[27] TIP4P/2005 is a rigid four site model which consists of three fixed point charges and one Lennard-Jones (LJ) center.[28] The three point-charges are placed at the oxygen and hydrogen atom positions, respectively. Specifically, oxygen and hydrogen atoms are assigned partial charges of q_O = -1.1128e and q_H = 0.5564e. The other site, often called the M site, is coplanar with the O and H sites and is located at the bisector of the H–O–H angle. The O–H distance and H–O–H angle are fixed at 0.9572 Å and 104.52°, respectively using SHAKE algorithm.[29] A particle-particle, particle-mesh (PPPM) was utilized to

correct the long-range electrostatic interactions.[30] LJ interactions were calculated between the wall molecules and the oxygen atoms of liquid water. We used the truncated LJ (12-6) potential to model the van der Waals interactions as follows:

$$V_{\text{truncated}}(r_{ij}) = 4\varepsilon\left[\left(\left(\frac{\sigma}{r_{ij}}\right)^{12} - \left(\frac{\sigma}{r_{ij}}\right)^{6}\right) - \left(\left(\frac{\sigma}{r_c}\right)^{12} - \left(\frac{\sigma}{r_c}\right)^{6}\right)\right] \quad (3)$$

where ε is the depth of the potential well, σ is the molecular diameter, r_{ij} is the intermolecular distance, and r_c is the cut-off distance. The intermolecular forces were truncated at a cut-off of 10.0 Å. The many-body potential embedded atom method (EAM), which describes the total energy of a metal by calculating the embedding energy as a function of the atomic electron density, was used to model the intermolecular forces between Au-Ag molecules. For the wettability of homogenous gold and homogeneous silver substrates, it is known that homogenous gold is more hydrophilic than homogenous silver. The experimentally reported contact angle values are 40°[31] and 72.8°,[32] respectively. As a result, we utilized the gold/water and silver/water interaction parameters which correctly reproduced the experimental water contact angles for the gold surface and the silver surface. Specifically, $\varepsilon_{\text{Au-O}}$ = 1.66 $\varepsilon_{\text{O-O}}$ = 0.013331908 eV, $\sigma_{\text{Au-O}}$ = 3.59645 Å, $\varepsilon_{\text{Ag-O}}$ = 2.0 $\varepsilon_{\text{O-O}}$= 0.0166254 eV, and $\sigma_{\text{Ag-O}}$ = 2.85495 Å.

All of the simulations were started from the Maxwell-Boltzmann velocity distribution for all molecules at 300 K. The periodic boundary condition was applied in all directions. The outermost layer of the substrate was fixed to the keep the volume of the simulation domain constant while the inner layers were left to vibrate normally. The NVT (constant number of molecules, constant volume, and constant temperature) ensemble was used initially with a Nose-Hoover thermostat, which maintained the system at 300 K. The time duration of the NVT ensemble was 1.0 ns to ensure that the system reached isothermal steady state. The NVE (constant number of molecules, constant volume, and constant energy) ensemble was then used and the duration of the NVE ensemble was 4.0 ns to ensure that the system reached the equilibrium state. Time averaging data of the desired values was performed over the last 2 ns of the NVE. For the contact angle measurement, the simulation domain was divided into three-dimensional bin structures to get center-of-mass droplet contour. For the density, stress, and surface tension calculations, the computational domain was divided into slab bins in the z directions, as shown in Fig. 1(c). This bin sizes were chosen to ensure that the data are collected properly.[3] Newton's equations of motion were integrated using the Verlet algorithm with a simulation time step of 1.0 femtosecond (fs). All simulations were performed using LAMMPS.[33]

The stress tensors of water include both kinetic and virial stresses in which the kinetic component represents the contributions from the linear momentum of particles whereas the virial component is the contributions from intermolecular forces between the particles. Also, because we worked with water, which has a complex molecular structure, the internal forces of the bonds and angles of water molecules must also be accounted for. The stress tensors were calculated based on the following formula:

$$S_{\alpha\beta} = -\left(mv_\alpha v_\beta + \frac{1}{2}\sum_{n=1}^{N_p}(r_{1\alpha}F_{1\beta} + r_{2\alpha}F_{2\beta}) + \frac{1}{2}\sum_{n=1}^{N_b}(r_{1\alpha}F_{1\beta} + r_{2\alpha}F_{2\beta}) + \frac{1}{3}\sum_{n=1}^{N_a}(r_{1\alpha}F_{1\beta} + r_{2\alpha}F_{2\beta} + r_{3\alpha}F_{3\beta}) + K_{\text{space}}(r_{i\alpha}, r_{i\beta}) + \sum_{n=1}^{N_f}(r_{i\alpha}, r_{i\beta})\right), \quad (4)$$

where the first term on the right-hand side is the kinetic component, in which m is the atomic mass of particle i and v_α and v_β are the velocity components of particle i in the α and β directions, respectively. The second, third, fourth, and fifth terms are the virial components. The second term is a pairwise energy contribution where n loops over the N_p neighbors of atom i, r_1 and r_2 are the positions, and F_1 and F_2 are the forces of the two atoms in the pairwise interaction. The third and fourth terms are the bond and angle contributions for the N_b bonds and N_a angle, respectively, of which atom i is part of. The K_{space} term is the contribution from the long-range Coulombic interactions for the PPPM solver. Finally, the fifth term is the SHAKE internal constraint force applied to particle i via the N_f fixes. The output stress values from LAMMPS are the per-atom array values which are a product of

the stress and volume units. Therefore, the actual local stress tensor in each bin was determined by dividing the total per-atom stress tensor by the volume of each bin using the following formula:

$$S_{\alpha\beta,\mathrm{bin}} = \frac{S_{\alpha\beta} \times N_{\mathrm{a}}}{V_{\mathrm{bin}}} \tag{5}$$

where $S_{\alpha\beta,\mathrm{bin}}$ is the actual local stress in a bin, N_{a} is the number of atoms per bin, and $V_{\mathrm{bin}} = L_x \times L_y \times \Delta z$, where L_x, L_y, and Δz are the dimensions of each bin in the x, y, and z directions, respectively.

III. RESULTS AND DISCUSSION

A. Density and normal stress distributions

The typical density profiles of a water in contact with the gold-silver striped substrate with gold surface fractions of 0.125, 0.5, and 0.875 are shown in Fig. 2(a). Density layering of the water molecules with two distinct peaks was observed on the substrate and it became more profound with increasing gold surface fraction. This kind of dynamic structure of fluid molecules near solid surface at the nanoscale is a well-known phenomenon and was reported in some significant experiments[34–37] and simulations.[38,39] The density build-up near the substrate-water interface was due to the fact that the surface forces are more dominant in the substrate-water interface than the water-water forces, which leads to the attraction of more water molecules to the substrate-water interface. The density values converged to the constant water density of 0.998 g/cm^3 after a distance of approximately 11.5 Å away from the substrate depending on the surface fractions. It was observed that the density peaks increased with increasing surface fraction of gold in the substrate as shown in Fig. 2(b). Beside the z-direction density profiles, the typical density contour in the y-z plane passing through the center of mass of a water droplet on a gold-silver striped substrate shown in Fig. 2(c) also helped to intuitively

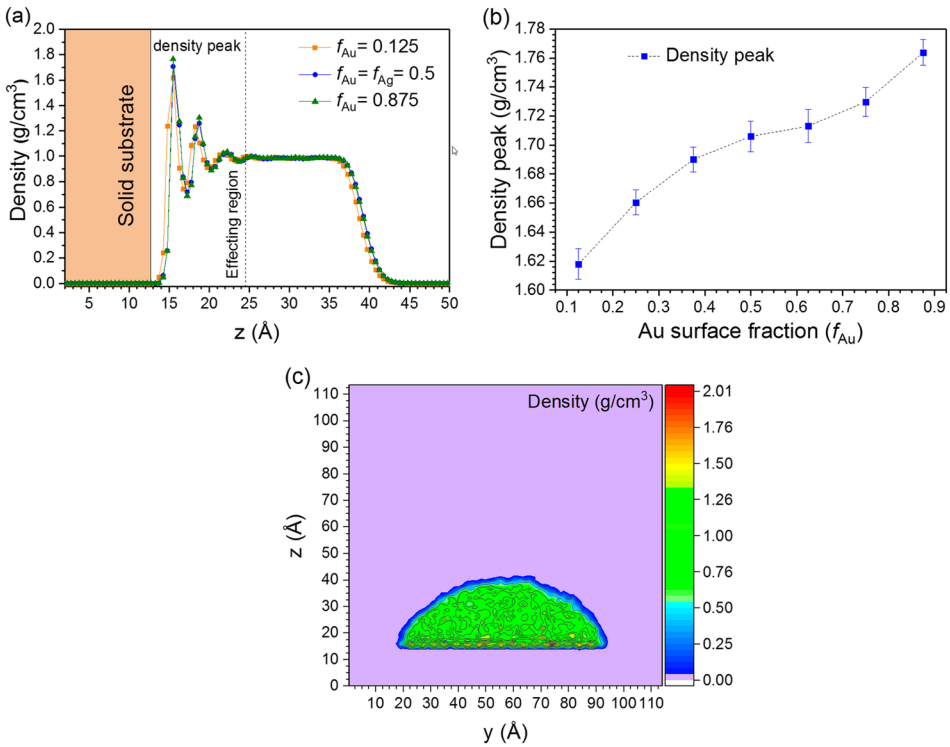

FIG. 2. Typical density profiles of water along the z direction for gold surface tensions of 0.125, 0.5, and 0.875 (a). Density peaks of water near the substrate-water interface for the different patterns of the gold-silver striped substrate for gold surface fractions of 0.125, 0.25, 0.375, 0.5, 0.625, 0.75, and 0.875 (b). Typical density contours in the z-y plane (parallel to stripes) for $f_{\mathrm{Ag}} = f_{\mathrm{Au}} = 0.5$ (c).

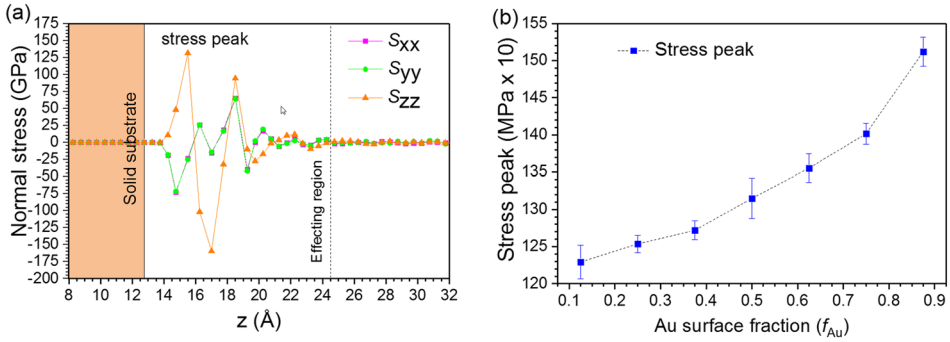

FIG. 3. Typical distributions of normal stress components along the z direction for the case of $f_{Ag} = f_{Au} = 0.5$ (a). Normal stress peaks of water near the substrate-water interface for the different patterns of the gold-silver striped substrate for gold surface fractions of 0.125, 0.25, 0.375, 0.5, 0.625, 0.75, and 0.875 (b).

express the behavior of water in the effecting region and bulk region of the water droplet. In a similar manner, we also concentrated on the distribution of the normal stresses of water in contact with the different patterns of the gold-silver striped substrate. S_{xx}, S_{yy}, and S_{zz} are denoted as the three mutually orthogonal components of the normal stress tensor acting along the x, y, and z directions of the simulation domain, respectively. The typical normal stress distribution in the case of equal gold and silver surface fractions is shown in Fig. 3(a). Like the behavior of the liquid water density distribution near the gold-silver striped substrate surface, a dominant stress peak and a much weaker second stress peak indicate the onset of density layering effects on the normal stress distribution. The normal stress values converged to a constant value after a distance of approximately 11.5 Å away from the substrate depending on the surface fractions. We defined the region away from the substrate's surface to the starting point of convergence of both density and normal stress components as the "effecting region" of the water near the solid-liquid interface. It was also observed that the normal stress peak increased when the fraction of gold in the substrate increased as in Fig. 3(b).

The similarity in the near-surface behavior of the water density and normal stress distribution reinforce the dominant role of the solid substrate in inducing fluctuating behavior of a liquid near the solid-liquid interface. This phenomenon is attributed to the fact that as the portion of gold in the substrate became more and more dominant, the intermolecular interactions between the substrate and water increased. This allowed the virial stresses at the interface to increase because virial stresses are directly related to intermolecular interactions between molecules. In light of this observation, we concluded that the increasing gold content or a stronger wetting material fraction in the chemically heterogeneous striped substrate leads to the increase in the wettability of the whole substrate, which strongly affects the momentum transport at the solid-liquid interface.

B. Surface tensions

Surface tension values at the boundaries between the solid-liquid, solid-vapor, and liquid-vapor interfaces of a droplet are expected to further explain the influence of the chemically heterogeneous striped substrate on the water droplet. The surface tension values were calculated using Bakker's equation.[40] Bakker's equation is a method to directly calculate the surface tensions of flat interfaces and runs via an integral over components of the pressure tensor obtained in a simulation. The equation is applicable to a structured or structureless wall in which the wall is located at $z = 0$ and the fluid at $z > 0$. In our case, all the interfaces are flat, so Bakker's equation is fully applicable to calculating the corresponding surface tensions. The equation is provided as follows:

$$\gamma = \int [S_N(z) - S_T(z)]dz \tag{6}$$

where γ is can be any of the three surface tensions and $S_N(z)$ and $S_T(z)$ are the stress components normal and tangential to an interface, respectively. $S_N(z)$ and $S_T(z)$ are obtained from the local normal stress components of the local Δz regions shown in Fig. 1(b). As such, for each local Δz region,

$S_N = S_{zz}$, $S_T = ½(S_{xx} + S_{yy})$, and the value of each local normal stress component (S_{xx}, or S_{yy}, or S_{zz}) of a Δz region can be calculated using Eq. (5). The integration range for the solid-liquid surface is along the z direction and bounded inside the "effecting region" of the normal stress, that for solid-vapor surface tension is from outside of the liquid region to the end of the simulation box,[41] and that for liquid-vapor surface tension is from the substrate surface to liquid-vapor boundary.[27] The liquid-vapor boundary is defined as the point where the density goes to zero with a rapid decrease away from the substrate.

The liquid-vapor, solid-liquid, and solid-vapor surface tensions obtained for the different gold and silver surface fractions are shown in Fig. 4. Interestingly, it is shown in Fig. 4(a) that the liquid-vapor surface tension did not change significantly for the different gold and silver fractions. The liquid-vapor surface tension fluctuated around the average value of 71.2 mN/m. This reveals that the liquid-vapor surface tension was not affected by the chemically heterogeneous striped substrate even if the substrate composition has a higher or lower amount of gold in it. Our results are consistent with the liquid-vapor surface tension values obtained from experiments[42–44] and from MD simulations using TIP4P/2005 model for pure water in which PPPM method was used.[27,45] Therefore, we can conclude that liquid-vapor surface tension of water is nearly constant and is not dependent on the chemical complexity of a solid substrate. Similarly, the solid-vapor surface tension was found to be unchanged and equal to zero for the different patterns of the gold-silver striped substrate, as shown in Fig. 4(b). This suggests that the surface tension at the boundary between a solid substrate and water vapor can be negligible. However, significantly, the solid-liquid surface tension was found to nonlinearly decrease with increasing gold surface fraction. This important result can be understood as when the gold fraction in the substrate is increased, at the substrate-water interface, the interaction between solid molecules and water molecules becomes more dominant. In other words, the interaction between the water molecules themselves becomes less dominant. This critical attenuation of the water-water interaction dominancy led to the decrease of the surface tension at the substrate-water boundary.

In light of the observed solid-liquid surface tension behavior, we attempted to develop an empirical approximation for predicting the solid-liquid surface tension of a water droplet resting on a chemically heterogeneous striped substrate based on the surface fractions of the constituting materials of the substrate (material 1 and material 2) and the solid-liquid surface tension values of the corresponding homogenous substrates as follows:

$$\gamma_{SL}^{(h)} = 6.7(\gamma_{SL1} + \gamma_{SL2}) \exp(-1.82\alpha) \tag{7}$$

Here, $\gamma_{SL}^{(h)}$ is the solid-liquid surface tension of the droplet resting on the chemically heterogeneous striped surface, h stands for "heterogeneous", γ_{SL1} and γ_{SL2} are the solid-liquid surface tensions of the droplet resting on the homogeneous material 1 and material 2, respectively, α is defined as the "general" solid-liquid interaction strength ratio of the chemically heterogeneous striped substrate

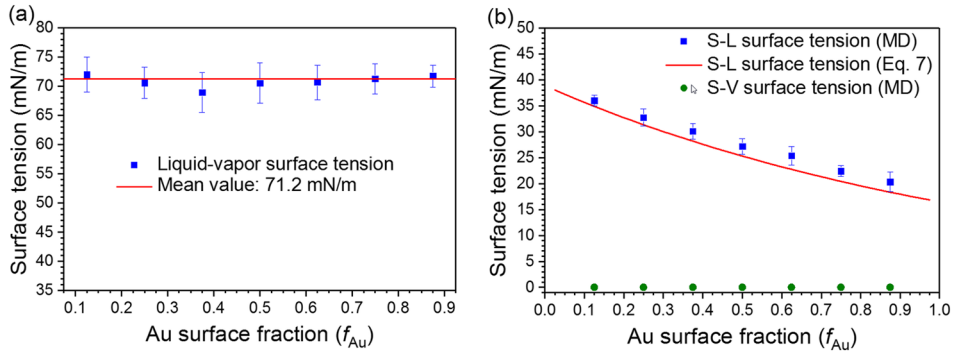

FIG. 4. Liquid-vapor surface tension of the water droplet for gold surface fractions of 0.125, 0.25, 0.375, 0.5, 0.625, 0.75, and 0.875 (a). Solid-liquid tensions obtained from MD calculation via Eq. (6) (blue dots), solid-liquid surface tension predictions obtained from Eq. (7) (red line), and solid-vapor surface tensions (green dots) obtained from MD calculation via Eq. (6) of the water droplet for gold surface fractions of 0.125, 0.25, 0.375, 0.5, 0.625, 0.75, and 0.875 (b).

with water and $\alpha = f_1\alpha_1 + f_2\alpha_2$ where α_1 and α_2 ($\alpha_i = 1 + \cos\theta_i$) are defined as the "general" solid-liquid interaction strength ratio of material 1 and material 2 with water, respectively, and f_1 and f_2 are the surface fractions of material 1 and material 2, respectively. According the definition of α, the greater the surface fraction of a material in the substrate composition, the more dominant its role in contributing the general solid-liquid interaction strength ratio value of its corresponding homogeneous substrate to that of the heterogeneous striped substrate. In our study, this definition was used because the specific solid-liquid interaction strength ratios of gold-water and silver-water in MD simulations do not represent the wettability contrast between gold and silver well. As provided in Section II, $\varepsilon_{Au\text{-}O}/\varepsilon_{O\text{-}O} = 1.66$ and $\varepsilon_{Ag\text{-}O}/\varepsilon_{O\text{-}O} = 2.0$ where as the wettability of gold is higher than that of silver. This uncorrelated relationship between interaction parameters and contact angles for different materials was also shown by Vo *et al.*[46] Thus, we need a general parameter which is able to illustrate not only the solid-liquid interaction strength ratio value but also the wettability contrast between the materials. Due to the fact that the cosine of the contact angle formed between a water droplet and a solid substrate is proportionally related to the wettability of a solid substrate, the cosine value can be utilized to represent for a general solid-liquid interaction strength ratio between the solid substrate and water. However, when θ_i is greater than 90^o, $\cos\theta_i$ is a negative value which is not appropriate to a ratio value. Thus, an offset value of 1.0 was added to $\cos\theta_i$ to form the term α_i which is able to represent for the general solid-liquid interaction strength ratio between the solid substrate and water. As such, when θ_i goes from 0^o to 180^o, α_i decreases from 2.0 to 0.0 and this properly shows that general solid-liquid interaction strength ratio decreases with increasing contact angle value. The definition of α_i helps us characterize the general solid-liquid interaction strength ratio of a solid substrate with a water droplet resting on the substrate only based on the contact angle value of the droplet without concerning about the specific value of solid-liquid interaction ratio of the substrate and water in MD simulations. In our case, the general solid-liquid interaction strength ratios of pure gold and silver substrates with water are 1.765 and 1.294, respectively. In addition, in order to predict the solid-liquid surface tension of a water droplet resting on the chemically heterogeneous striped substrate using Eq. (7), all of the relevant solid-liquid surface tensions of the corresponding homogeneous substrates were obtained. The solid-liquid surface tension predictions of the water droplet resting on different patterns of the gold-silver striped substrate are shown in Fig. 4(b). Good agreement is observed between the calculated and predicted values. Also, it is seen that the solid-liquid surface tension decreases exponentially with increasing gold surface fraction. In other words, the solid-liquid surface fraction decreases exponentially as the general solid-liquid interaction strength ratio increases. Our result is similar to the phenomenon relevant to solid-liquid surface energy shown in the study of Kuna *et al.*[47] By using atomic force microscopy (AFM) measurements and MD simulations, the authors demonstrated that the solid-liquid surface energy at the solid-liquid interface of chemically heterogeneous surfaces having domains commensurate in size with solvent molecules is non-linearly proportional to the surface composition. Recently, the effects of nanoscale chemical heterogeneity on hydrophobic interaction of surfaces[48] and binding energy of ion head groups (Gdn-Gho)[49] were also revealed by AFM measurements. Moreover, the nonlinear exponential behavior of the solid-liquid surface tension with respect to the general solid-liquid interaction strength ratio is similar to the reported behavior of the interface thermal resistance of a solid wall with respect to the interaction strength ratio between the wall and a liquid.[2,50–52] It was shown that exponential curve fit is the best for physical phenomena on van der Waals interfaces. This kind of exponential behavior is generally caused by the important role of 6-12 Lennard-Jones potential interactions between solid and liquid molecules.

C. Contact angle measurement and prediction model for a droplet resting on a chemically heterogeneous striped substrate at the nanoscale

In this study, the contact angles of the water droplet were measured parallel to the stripes to observe the combined effect of the different wetting materials which constitute the substrate. The contact angle of water droplet in the direction perpendicular to the stripe's direction was not considered. In the perpendicular view, it was not possible to obtain the correct contact angle of a water droplet because at its equilibrium position, the droplet contact line can reside more or less on gold or silver. In the direction parallel to the stripes, the droplet contour was expected to be strongly

influenced by the rapidly varying wetting nature of the substrate. As such, the parallel contact angle is believed to be mostly determined by the chemical composition of the surface.[19] Hereby, the term "contact angle" is the parallel contact angle. A contact angle was measured based on the density contour of the y-z plane parallel with the stripes and passing through the droplet center. The droplet boundary was determined as the point at which the density is half that of bulk water (0.5 g/cm^3). The center-of-mass contour of the droplet is circular except in the near wall region. Then, a circle was drawn along the boundary from the points 11.5 Å above the substrate to avoid the effects of density fluctuation at the solid-liquid interface. Finally, the contact angle, θ, of the water droplet at the equilibrium state was determined using a simple geometric formula reported previously.[7]

First, we attempted to verify the applicability of Young's equation (Eq. 2) in predicting the contact angle of a chemically heterogeneous substrate at the nanoscale although its use is well-known for determining the contact angle at the macro-scale. Based on the values of the liquid-vapor, solid-liquid, and solid-vapor surface tensions obtained previously, we directly calculated the contact angle using Young's equation. The contact angles obtained from Young's equation for the different gold surface fractions are shown in Fig. 6(a) and summarized in Table I. It can be seen that the contact angles calculated using Young's equation were much higher than those obtained using the density contour method in the MD simulations. This result proves that Young's equation is not completely valid in predicting the contact angle of a chemically heterogeneous substrate at the nanoscale.

Second, we also verified the applicability of the CB model (Eq. 1) at the nanoscale. In the first set of MD simulations, we obtained a contact angle of 40.1^o for the water droplet on the pure gold substrate and 72.8^o for the water droplet on the pure silver substrate. These contact angles are in good agreement with the experimental values mentioned in the simulation details and they are the key parameters used for calculating and verifying the contact angles obtained using the CB model. As shown in Table I, poor agreement was obtained between the CB predictions and the MD measurement data. The water contact angles for all of the different gold fractions in the gold-silver striped substrate at the nanoscale were lower than the predictions of the CB model.

The breakdown of the CB model in predicting the contact angle of water droplets at the nanoscale can be explained. It is noticeable that the CB model only correctly predicts the effect of substrate heterogeneity on the equilibrium contact angle of chemically heterogeneous substrates at the macro-scale where the effect of line tension is usually ignorable due to the large size of droplets. However, at the nanoscale, the size of droplets is nanometer-sized, so the effect of line tension at the three-phase contact line cannot be neglected. For a homogeneous substrate, the important influence of the line tension at the three-phase contact line due to the droplet size effect on the free energy of a nanometer-sized droplet resting on that substrate is described by the modified Young's equation:[53]

$$\gamma_{SV} = \gamma_{SL} + \gamma_{LV} \cos\theta + \frac{\tau}{r} \tag{8}$$

where γ_{SV}, γ_{SL}, and γ_{LV} are the solid-vapor, solid-liquid, and liquid-vapor surface tensions at the boundaries between the solid-vapor, solid-liquid, and liquid-vapor interfaces, respectively, τ is the line tension at the three-phase contact line, and r is the drop base radius. Therefore, in predicting the contact angle of chemically heterogeneous substrates, the effect of the substrate heterogeneity on the line tension at the three-phase contact line must also be considered.[54] Based on the changing

TABLE I. Summary of the contact angles (degree) of a water droplet resting on the gold-silver striped substrates with different gold and silver surface fractions using different methods.

f_{Au}	f_{Ag}	Young's Eq.	Cassie-Baxter Eq.	MD Simulation	Eq. (11)
0.125	0.875	120.4	69.2	66.2	64.5
0.25	0.75	117.4	65.6	59.6	60.0
0.375	0.625	114.9	61.8	55.2	55.7
0.5	0.5	111.4	57.9	50.5	51.5
0.625	0.375	110.8	53.9	47.1	47.4
0.75	0.25	108.3	49.6	43.6	43.4
0.875	0.125	106.5	45.0	42.1	39.5

tendency of the contact angle with different surface fractions of gold and silver, we expect that the line tension value should be affected by the surface fractions. In light of this, we developed a linear approximation for predicting the line tension of a nanometer-sized droplet resting on a chemically heterogeneous striped substrate comprised of material 1 and material 2 based on the surface fractions of the materials as follows:

$$\tau^{(h)} = f_1\tau_1 + f_2\tau_2 \tag{9}$$

where $\tau^{(h)}$ is the line tension of the droplet resting on the chemically heterogeneous striped substrate, h stands for "heterogeneous", and τ_1 and τ_2 are the line tensions of the droplet resting on homogeneous material 1 and material 2, respectively. As described in the equation, the greater the surface fraction of a material in the substrate composition, the more dominant its role in affecting the line tension value and the closer the line tension value is to that of the corresponding homogeneous substrate. In addition, when the role of line tension is taken into consideration, the value of the drop base radius shaped by the droplet and the solid substrate must also be considered. Due to the effects of the differently wetting stripes, the contact line at the drop edge which is perpendicular to the stripes can be distorted or stretched. However, because the stripes are molecular-sized in width and rapidly changing, the contact line distortion is negligible. Thus, we assume that the three-phase contact line affected by these stripes was circular with the drop base radius approximated from the two radiuses obtained from the two homogeneous substrates based on a linear approximation as follows:

$$r^{(h)} = f_1 r_1 + f_2 r_2 \tag{10}$$

where $r^{(h)}$ is the drop base radius of the water droplet resting on a chemically heterogeneous striped substrate, h stands for "heterogeneous", and r_1 and r_2 are drop base radiuses of droplets resting on homogeneous material 1 and material 2, respectively. Based on this approximation, it is reasonable that the greater the surface fraction of the more wetting material in the substrate composition is, the larger the drop base radius of the water droplet or the more the water droplet is spread out to the direction parallel to the stripes.

In order to predict the line tension and drop base radius of a water droplet resting on a chemically heterogeneous striped substrate using Eq. (9) and Eq. (10), all of the line tensions and drop base radiuses of the corresponding homogeneous substrates must be available. In our study, the drop base radiuses of the water droplet resting on homogeneous gold and silver substrates were obtained through MD simulations. The line tension values of the homogeneous gold and silver substrate were then calculated using Eq. (8) utilizing the measured drop base radiuses and the available surface tension values obtained previously. The line tension values of the homogeneous gold and homogeneous silver substrates are -2.98×10^{-10} N and -2.17×10^{-10} N, respectively. The calculated line tension values are consistent with the order of magnitude and sign of other results obtained in experimental measurements[51,55,56] and simulations.[7,57,58] Based on the values of the line tension and drop base radiuses obtained from the homogenous gold and homogeneous silver substrates, the predicted values of line tension and drop base radius obtained using Eq. (9) and Eq. (10) are shown in Fig. 6(b) and 6(c), respectively.

Concurrently, in order to verify the validity of Eq. (9) and Eq. (10) in predicting the line tension and drop base radius values, we attempted to obtain the line tension and drop base radius values from the MD simulation data for comparison with the predicted values obtained from Eq. (9) and Eq. (10). We measured the base radius of the droplet part belonging to the center-of-mass frame parallel to the stripes. Each reported radius value is the averaged value of the corresponding values at equilibrium. Fig. 5 illustrates the droplet base radius measurement method using center-of-mass frames. By substituting all of the MD measured values of the drop base radius together with the available solid-liquid, solid-vapor, and liquid-vapor surface tension values obtained previously into Eq. (8), the line tension values at the three-phase contact line of the water droplet and gold-silver striped substrate for the different gold and silver surface fractions were obtained. It is shown in Fig. 6(b) and 6(c) that the values of the line tensions and drop base radiuses predicted by Eq. (9) and Eq. (10) are in good agreement with those values obtained via Eq. (8) and MD measurement. In both prediction and MD calculation, the base radius and the magnitude of the line tension increased with increasing gold portion in the substrate. This good result confirmed the reliability of our prediction methods.

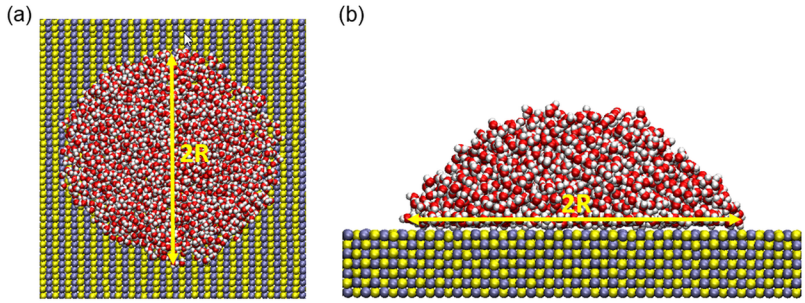

FIG. 5. Schematic for drop base radius measurement method using center-of-mass frames: top view (a), side view (b).

Most importantly, taking into consideration the essential role of all surface tensions, line tensions, and base radiuses, we proposed and method to predict the contact angle of a nanometer-sized droplet resting on a chemically heterogeneous striped substrate compose of two different materials by extending the modified Young's equation (MYE) as follows:

$$\cos\theta^{(\mathrm{h})} = \frac{\gamma_{\mathrm{SV}} - \gamma_{\mathrm{SL}}^{(\mathrm{h})}}{\gamma_{\mathrm{LV}}} - \frac{\tau^{(\mathrm{h})}}{\gamma_{\mathrm{LV}} r^{(\mathrm{h})}} \tag{11}$$

where $\gamma_{\mathrm{SL}}^{(h)}$, $\tau^{(\mathrm{h})}$, and $r^{(\mathrm{h})}$ are the quantities obtained from Eq. (7), Eq. (9), and Eq. (10), respectively, h stands for "heterogeneous", and γ_{SV} and γ_{LV} are the solid-vapor and liquid-vapor surface tensions, respectively, which are unchanged with the substrate complexity. According to this equation, the influences of the substrate composition represented by the surface fraction parameters on the surface tensions and line tension are important in shaping the contact angle value. Using all of the predicted surface tensions, line tensions, and base radiuses, we predicted the water contact angle of the water

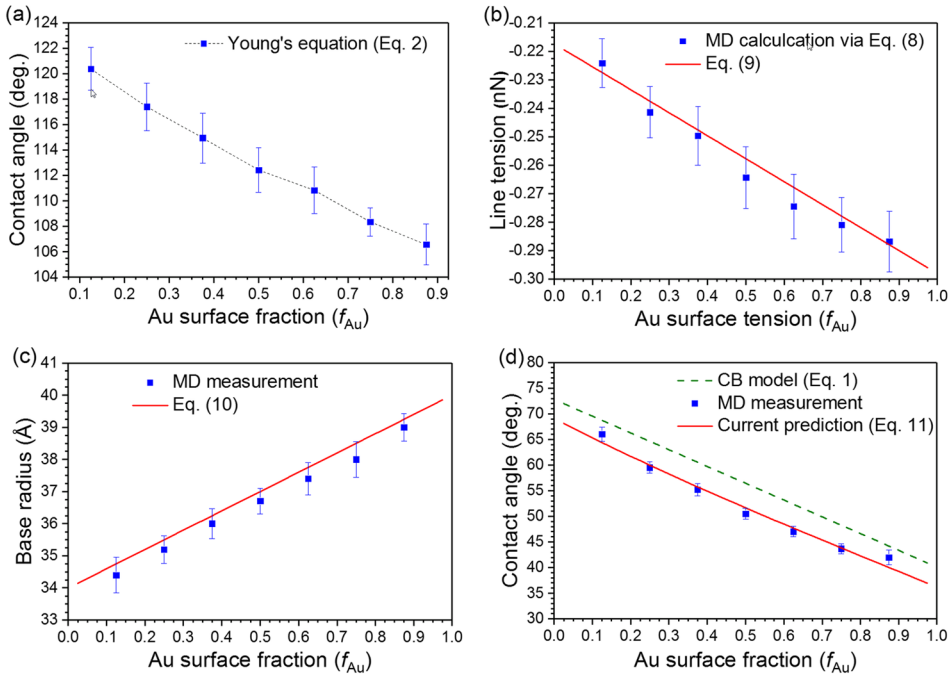

FIG. 6. Contact angles obtained from Young's equation (Eq. 2) using all of the calculated MD surface tensions (a). Comparison of the line tensions obtained from MD calculation (blue dots) using Eq. (8) and predictions using Eq. (9) (red line) (b). Comparison of the drop base radiuses obtained from MD measurement (blue dots) and prediction using Eq. (10) (red line) (c). Contact angles obtained from the CB model (dashed line), MD measurement (blue dots), and our prediction method using Eq. (11) (red line) with respect to the gold surface fraction (d).

droplet resting on the different gold-silver striped substrate patterns using the extended MYE, as shown in Fig. 6(d). Good agreement was observed between the contact angles obtained from the extended MYE and the contact angles measured using the density contour method. It can be recognized that as compared to the CB model as well as Young's equation, the extended MYE did a better job in predicting the value of contact angle as well as the tendency as a result of including the significant effect of line tension on the contact angle value of the gold-silver striped substrate at the nanoscale. This result confirmed that together with the important role of surface tensions, the role of line tension in determining the contact angle of chemically heterogeneous substrates at the nanoscale is indispensable. Therefore, the proposed extended MYE is believed to clearly represent the critical role of line tension in affecting the contact angle of a liquid droplet resting on a chemically heterogeneous striped substrate at the nanoscale. In addition, the equation provides a good method to predict contact angles for use in other research in the same field.

IV. CONCLUSIONS

In this study, we performed a thorough investigation of the wettability of a chemically heterogeneous striped substrate at the nanoscale using MD simulations. The effects of the chemically heterogeneous striped substrate comprised of gold and silver stripes on the density distribution, normal stress distribution, surface tensions at three phase boundaries, and the contact angle of a water droplet were evaluated. Significant influences of the chemically heterogeneous striped substrate on the density and normal stress behavior near the substrate-water interface were explicitly shown. Further investigation of the surface tensions at the liquid-vapor, solid-vapor, and solid-liquid boundaries of the water droplet with the chemically heterogeneous striped substrate revealed that the liquid-vapor surface tension of a water droplet is constant regardless of the complexity of the chemically heterogeneous striped substrate. Similarly, the solid-vapor surface tension was found to be zero for all of the different patterns of the chemically heterogeneous striped substrate. Importantly, we observed that the solid-liquid surface tension decreased exponentially with increasing surface fraction of the stronger wetting material (gold) in the chemically heterogeneous striped substrate. This phenomenon helped us affirm the role of the stronger wetting material (gold) in enhancing the intermolecular interactions between solid and liquid molecules at the substrate-water interface. Finally, the invalidity of Young's equation and the CB model in predicting the contact angle of a chemically heterogeneous striped substrate at the nanoscale was carefully confirmed. In light of this observation, by taking into consideration the indispensable effects of line tension on shaping the contact angle of a nanometer-sized water droplet resting on the chemically heterogeneous striped substrate, we successfully proposed a method for predicting the contact angle for that substrate at the nanoscale. The values obtained from the proposed equation demonstrate that the new prediction method does a good job of predicting the value and the changing tendency of the contact angle as the portions of the constituting materials in the substrate composition vary. We are optimistic that the extended MYE will be applicable in predicting the wettability of chemically heterogeneous striped substrates utilizing the contact angle value in other nano-scale fluidic research.

ACKNOWLEDGMENTS

This research was supported by Basic Science Research Program through the National Research Foundation of Korea (NRF) funded by the Ministry of Education (NRF-2016R1D1A1B03932737).

[1] D. G. Cahill, W. K. Ford, K. E. Goodson, G. D. Mahan, A. Majumdar, H. J. Maris, R. Merlin, and S. R. Phillpot, J. Appl. Phys. **93**, 793 (2003).
[2] H. B. Kim, A. Beskok, and T. Cagin, J. Chem. Phys. **129**, 174701 (2008).
[3] H. B. Kim, A. Beskok, and T. Cagin, Microfluid. Nanofluid. **9**, 31 (2010).
[4] A. T. Pham, M. Barisik, and B. Kim, Int. J. Precis. Eng. Manuf. **15**, 323 (2014).
[5] A. T. Pham, M. Barisik, and B. Kim, J. Chem. Phys. **139**, 244702 (2013).
[6] T. Q. Vo and B. Kim, Sci. Rep. **6**, 033881 (2016).
[7] M. Barisik and A. Beskok, Mol. Simul. **39**, 700 (2013).
[8] T. Werder, J. H. Walther, R. L. Jaffe, T. Halicioglu, and P. Koumoutsakos, J. Phys. Chem. B **107**, 1345 (2003).
[9] S. Wang, Y. Zhang, N. Abidi, and L. Cabrales, Langmuir **25**, 11078 (2009).

[10] J. Rafiee, X. Mi, H. Gullapalli, A. V. Thomas, F. Yavari, Y. Shi, P. M. Ajayan, and N. A. Koratkar, Nat. Mater. **11**, 217 (2012).
[11] C. T. Nguyen and B. Kim, Int. J. Precis. Eng. Manuf. **17**, 503 (2016).
[12] J. Léopoldès, A. Dupuis, D. G. Bucknall, and J. M. Yeomans, Langmuir **19**, 9818 (2003).
[13] P. J. Rossky, Faraday Discuss. **146**, 13 (2010).
[14] T. P. Russel, T. Thurn-Albrecht, M. Tuominen, E. Huang, and C. J. Hawker, Macromol. Symp. **159**, 77 (2000).
[15] A. B. D. Cassie and S. Baxter, Trans. Faraday Soc. **40**, 546 (1944).
[16] A. B. D. Cassie, Discuss. Faraday Soc. **3**, 11 (1948).
[17] S. Brandon, N. Haimovich, E. Yeger, and A. Marmur, J. Colloid Interface Sci. **263**, 237 (2003).
[18] H. P. Jansen, O. Bliznyuk, E. S. Kooij, B. Poelsema, and H. J. W. Zandvliet, Langmuir **28**, 499 (2012).
[19] E. S. Kooij, H. P. Jansen, O. Bliznyuk, B. Poelsema, and H. J. W. Zandvliet, Colloids Surf., A **413**, 328 (2012).
[20] D. Bormashenko, Colloids Surf., A **324**, 47 (2008).
[21] X. Gao and L. Jiang, Nature **432**, 36 (2004).
[22] X. Q. Fang, X. Gao, Z. Wu, L. Jiang, and Q. S. Zheng, Langmuir **23**, 4892 (2007).
[23] M. Lundgren, N. L. Allan, and T. Cosgrove, Langmuir **23**, 1187 (2007).
[24] J. N. Israelachvili and M. L. Gee, Langmuir **5**, 288 (1989).
[25] J. D. Halverson, C. Maldarelli, A. Couzis, and J. Koplik, Soft Matter **6**, 1297 (2010).
[26] J. Wang, D. Bratko, and A. Luzar, PNAS **108**, 6374 (2011).
[27] C. Vega and E. De Miguel, J. Chem. Phys. **126**, 154707 (2007).
[28] J. L. F. Abascal and C. A. Vega, J. Chem. Phys. **123**, 234505 (2005).
[29] J. P. Ryckaert, G. Ciccotti, and H. J. C. Berendsen, J. Comput. Phys. **23**, 327 (1977).
[30] M. P. Allen and D. J. Tildesley, *Computer Simulation of Liquids* (Clarendon Press, New York, 1989) p. 385.
[31] T. Smith, J. Colloid Interface Sci. **75**, 51 (1980).
[32] J. Pacifico, K. Endo, S. Morgan, and P. Mulvaney, Langmuir **22**, 11072 (2006).
[33] S. Plimpton, J. Comp. Phys. **117**, 1 (1995).
[34] F. Heslot, N. Fraysse, and A. M. Cazabat, Nature **339**, 640 (1989).
[35] L. Cheng, P. Fenter, K. L. Nagy, M. L. Schlegel, and N. C. Sturchio, Phys. Rev. Lett. **87**, 156103 (2001).
[36] U. Raviv and J. Klein, Science **297**, 1540 (2002).
[37] E. Mamontov, C. J. Burnham, S. H. Chen, A. P. Moravsky, C. K. Loong, N. R. de Souza, and A. I. Kolesnikov, J. Chem. Phys. **124**, 194703 (2006).
[38] A. T. Celebi, M. Barisik, and A. Beskok, J. Chem. Phys. **147**, 164311 (2017).
[39] A. T. Celebi and A. Beskok, J. Phys. Chem. C **122**, 9699 (2018).
[40] M. J. P. Nijmeijer, C. Bruin, A. F. Bakker, and J. M. J. Van Leeuwen, Phys. Rev. A **42**, 6052 (1990).
[41] S. Nishida, D. Surblys, Y. Yamaguchi, K. Kuroda, M. Kagawa, T. Nakajima, and H. Fujimura, J. Chem. Phys. **140**, 074707 (2014).
[42] N. R. Pallas and Y. Harrison, Colloids Surf. **143**, 168 (1990).
[43] R. Breslow and T. Guo, Proc. Natl. Acad. Sci. USA **87**, 167 (1990).
[44] J. Songok, P. Salminen, and M. Toivakka, J. Colloid Interface Sci. **418**, 373 (2014).
[45] R. D. Mountain, J. Phys. Chem. B **113**, 482 (2009).
[46] T. Q. Vo, M. Barisik, and B. Kim, Phys. Rev. E **92**, 053009 (2015).
[47] J. J. Kuna, K. Voitchovsky, C. Singh, H. Jiang, S. Mwenifumbo, P. K. Ghorai, M. M. Stevens, S. C. Glotzer, and F. Stellacci, Nat. Mater. **8**, 837 (2009).
[48] C. D. Ma, C. Wang, C. Acevedo-Vélez, S. H. Gellman, and N. L. Abbott, Nature **517**, 347 (2015).
[49] S. Chen, Y. Itoh, T. Masuda, S. Shimizu, J. Zhao, J. Ma, S. Nakamura, K. Okuro, H. Noguchi, K. Uosaki, and T. Aida, Science **348**, 555 (2015).
[50] L. Xue, P. Keblinski, S. R. Phillpot, S. U.-S. Choi, and J. A. Eastman, J. Chem. Phys. **118**, 337 (2003).
[51] J. L. Barrat and F. Chiaruttini, Mol. Phys. **101**, 1605 (2003).
[52] S. Murad and I. K. Puri, Chem. Phys. Lett. **467**, 110 (2008).
[53] J. Y. Wang, S. Betelu, and B. M. Law, Phys. Rev. E **63**, 031601 (2001).
[54] J. Drelich and J. D. Miller, Part. Sci. Technol. **10**, 1 (1992).
[55] T. Pompe and S. Herminghaus, Phys. Rev. Lett. **85**, 1930 (2000).
[56] J. K. Berg, C. M. Weber, and H. Riegler, Phys. Rev. Lett. **105**, 07610 (2010).
[57] J. H. Weijs, A. Marchand, B. Andreotti, D. Lohse, and J. H. Snoeijer, Phys. Fluids **23**, 022001 (2011).
[58] M. Shao, J. Wang, and X. Zhou, Sci. Rep. **5**, 1 (2015).